View metadata, citation and similar papers at core.ac.uk
brought to you by CORE
provided by Elsevier - Publisher Connector

Biophysical Journal Volume 78 April 2000 1703–1713

Two-Dimensional Fluorescence Intensity Distribution Analysis: Theory and Applications

Peet Kask,*† Kaupo Palo,* Nicolas Fay,* Leif Brand,* Ülo Mets,* Dirk Ullmann,* Joern Jungmann,* Johannes Pschorr,* and Karsten Gall*
*EVOTEC BioSystems AG, D-22525 Hamburg, Germany, and †Institute of Experimental Biology, Harku 76902, Estonia

ABSTRACT A method of sample analysis is presented which is based on fitting a joint distribution of photon count numbers. In experiments, fluorescence from a microscopic volume containing a fluctuating number of molecules is monitored by two detectors, using a confocal microscope. The two detectors may have different polarizational or spectral responses. Concentrations of fluorescent species together with two specific brightness values per species are determined. The two-dimensional fluorescence intensity distribution analysis (2D-FIDA), if used with a polarization cube, is a tool that is able to distinguish fluorescent species with different specific polarization ratios. As an example of polarization studies by 2D-FIDA, binding of 5′-(6-carboxytetramethylrhodamine) (TAMRA)-labeled theophylline to an anti-theophylline antibody has been studied. Alternatively, if two-color equipment is used, 2D-FIDA can determine concentrations and specific brightness values of fluorescent species corresponding to individual labels alone and their complex. As an example of two-color 2D-FIDA, binding of TAMRA-labeled somatostatin-14 to the human type-2 high-affinity somatostatin receptors present in stained vesicles has been studied. The presented method is unusually accurate among fluorescence fluctuation methods. It is well suited for monitoring a variety of molecular interactions, including receptors and ligands or antibodies and antigens.

INTRODUCTION

Fluorescence intensity distribution analysis (FIDA; Kask et al., 1999; independently Chen et al., 1999) has been recently developed as a complement to fluorescence correlation spectroscopy (FCS; Magde et al., 1972). The general idea of FIDA was introduced in 1990 (Qian and Elson, 1990a, b), but then realized as a less powerful method of moment analysis (MAFID). As in most common versions of FCS, in first realizations of MAFID and FIDA, a single detector was used to monitor fluorescence from a microscopic sample volume. However, fluorescence fluctuation spectroscopy does not have to be restricted to the use of a single detector. For different purposes, two detectors have been used in some applications of FCS. In the nanosecond time domain, the two-detector system has been applied simply because the dead time of the detector would otherwise not permit correlation studies on such a short time scale (Kask et al., 1985). In rotational correlation studies, two detectors have been used for monitoring light of different polarization, which helps one to distinguish fluctuations of light intensity due to rotational motion of particles from intensity fluctuations of other origin (Kask et al., 1989). Furthermore, in some cross-correlation studies two detectors monitor light of different colors originating from different fluorophores, enabling one to estimate to what extent two labeled molecules are bound to each other (Schwille et al., 1997). The present paper introduces the theory of FIDA with two detectors. The two-dimensional FIDA (2D-FIDA), if used with a polarization cube, is a tool that can distinguish fluorescent species with different specific polarization ratios. Alternatively, if two-color equipment is used, the 2D-FIDA can determine concentrations and specific brightness values of fluorescent species corresponding to individual labels as well as their complex.

The presented method is well suited for monitoring molecular interactions including receptors and ligands or antibodies and antigens, which are both of great relevance in the life sciences. The method is extremely accurate if the assay of interest can be designed with a significant contrast in specific brightness between bound and unbound states. Furthermore, it is characterized by single molecule sensitivity, the ability to resolve different species and determine their absolute concentrations, and to detect coincidences of different molecules in time and space. It is a homogeneous method, i.e., washing steps are not required. It is fast, well miniaturizable, and as a confocal technique, insensitive to surface adsorption. Therefore, 2D-FIDA is expected to find a wide variety of applications. Our pharmaceutical applications already cover the scale from detailed biochemical assay development to primary drug screening.

THEORY

The expected joint distribution of photon count numbers

To elaborate a simple theory that enables one to express the expected two-dimensional distribution of the number of photon counts, it is favorable to use the same assumptions used in one-dimensional FIDA and its predecessor, the moment analysis of photon count number distribution. The

Received for publication 8 September 1999 and in final form 12 January 2000.

Address reprint requests to Dr. Karsten Gall, EVOTEC BioSystems AG, Schnackenburgallee 114, D-22525 Hamburg, Germany. Tel.: 49-40-560-81-0; Fax: 49-40-560-81-222; E-mail: gall@evotec.de.

© 2000 by the Biophysical Society

0006-3495/00/04/1703/11 $2.00

assumptions are as follows. 1) Coordinates of particles are random and independent of each other; 2) contribution to fluorescence intensity from a particle can be expressed as a product of a specific brightness of the particle and a spatial brightness profile function characteristic of the optical equipment; and 3) a short counting time interval T is selected, during which the brightness of fluorescent particles does not significantly change due to translational diffusion.

We shall first express a joint distribution of count numbers from a single fluorescent species and a single small open volume element dV. The latter is a small fraction of the microscopic observable volume, where the spatial brightness is considered to be constant. Let us characterize the volume element by coordinates $\mathbf{r}$ and spatial brightness $B(\mathbf{r})$, and the fluorescent species by its specific brightness values q_1 and q_2. By q_1 and q_2 we have denoted the mean photon count rates by two detectors from a particle situated at a point where $B(\mathbf{r}) = 1$. The spatial brightness function describes the varying excitation and detection conditions across the observed volume. A convenient choice is to select a unit of B, as usual in FCS, by the equation $\chi_1 = \chi_2$, where $\chi_k = \int B^k(\mathbf{r}) d^3\mathbf{r}$. If the volume element contains m particles, then the expected mean photon count numbers per time interval T from the volume element are $mq_1TB(\mathbf{r})$ and $mq_2TB(\mathbf{r})$, while the joint distribution of the numbers of photon counts from m particles is Poissonian for both detectors independently:

$$P(n_1, n_2|m) = \frac{(mq_1TB(\mathbf{r}))^{n_1}}{n_1!} e^{-mq_1TB(\mathbf{r})} \frac{(mq_2TB(\mathbf{r}))^{n_2}}{n_2!} e^{-mq_2TB(\mathbf{r})}. \quad (1)$$

From the other side, under assumption 1), the distribution of the number of particles of a given species in the volume element is Poissonian with mean cdV, c denoting concentration:

$$P_{dV}(m) = \frac{(cdV)^m}{m!} e^{-cdV}. \quad (2)$$

The overall distribution of the number of photon counts from the volume element can be expressed using Eqs. 1 and 2:

$$\begin{aligned} P_{dV}(n_1, n_2) &= \sum_m P_{dV}(m) P(n_1, n_2|m) \\ &= \sum_m \frac{(cdV)^m}{m!} e^{-cdV} \frac{(mq_1TB(\mathbf{r}))^{n_1}}{n_1!} e^{-mq_1TB(\mathbf{r})} \\ &\quad \cdot \frac{(mq_2TB(\mathbf{r}))^{n_2}}{n_2!} e^{-mq_2TB(\mathbf{r})} \end{aligned} \quad (3)$$

As in 1D-FIDA, a useful representation of a distribution of the number of photon counts $P(n_1, n_2)$ is its generating function, defined as

$$G(\xi_1, \xi_2) = \sum_{n_1=0}^{\infty} \sum_{n_2=0}^{\infty} \xi_1^{n_1} \xi_2^{n_2} P(n_1, n_2). \quad (4)$$

The generating function of the distribution expressed by Eq. 3 can be written as

$$\begin{aligned} G_{dV}(\xi_1, \xi_2) &= e^{-cdV} \sum_m \frac{(cdV)^m}{m!} e^{-mq_1B(\mathbf{r})T} e^{-mq_2B(\mathbf{r})T} \\ &\quad \cdot \sum_{n_1} \frac{(m\xi_1 q_1 B(\mathbf{r})T)^{n_1}}{n_1!} \sum_{n_2} \frac{(m\xi_2 q_2 B(\mathbf{r})T)^{n_2}}{n_2!} \\ &= e^{-cdV} \sum_m \cdot \frac{\{cdV \exp[(\xi_1 - 1) q_1 B(\mathbf{r})T] \exp[(\xi_2 - 1) q_2 B(\mathbf{r})T]\}^m}{m!} \\ &= \exp[cdV(e^{(\xi_1 - 1)q_1B(\mathbf{r})T} e^{(\xi_2 - 1)q_2B(\mathbf{r})T} - 1)]. \end{aligned} \quad (5)$$

In particular, if one selects $\xi = e^{i\varphi}$, then the distribution $P(n_2, n_2)$ and its generating function $G(\varphi_1, \varphi_2)$ are interrelated by a two-dimensional Fourier transform. What makes the generating function attractive in photon count number distribution analysis is the additivity of its logarithm: logarithms of generating functions of photon count number distributions of independent sources, like different volume elements and different species, are simply added for the calculation of the combined distribution. Therefore, the generating function of the overall distribution of the number of photon counts can be expressed in a closed form:

$$\begin{aligned} G(\xi_1, \xi_2) = \exp[&(\xi_1 - 1)\lambda_1 T + (\xi_2 - 1)\lambda_2 T \\ &+ \sum_i c_i \int (e^{(\xi_1 - 1)q_{1i}TB(\mathbf{r})} e^{(\xi_2 - 1)q_{2i}TB(\mathbf{r})} - 1) d^3\mathbf{r}]. \end{aligned} \quad (6)$$

In this formula we have integrated a contribution from background count rates, λ_1 by detector 1 and λ_2 by detector 2, and contributions from different fluorescent species, denoted by the subscript i. Numeric integration according to Eq. 6 followed by a fast Fourier transform is to our knowledge the most efficient means to calculate the theoretical distribution $P(n_1, n_2)$ of a given sample (i.e., given concentrations and specific brightness values of fluorescent species).

The spatial brightness function

The spatial brightness function is accounted for through the spatial integration on the right side of Eq. 6. In the same way as in 1D-FIDA, the three-dimensional integration can be reduced to one dimension by replacing the three-dimensional coordinates $\mathbf{r}$ by a one-dimensional variable, a monotonic function of the spatial brightness $B(\mathbf{r})$. A convenient

choice of the variable is $x = \ln[B(0)/B(\mathbf{r})]$. A sufficiently flexible model of the one-dimensional spatial brightness profile is presented in the following expression:

$$\frac{dV}{dx} \propto x(1 + a_1x + a_2x^2). \quad (7)$$

(Note that Eq. 7 was introduced in FIDA as a means to obtain a sufficiently good fit between measured and calculated curves; the fit quality is indeed significantly better compared to what the Gaussian model with a rigid relationship $dV/dx \propto \sqrt{x}$ would yield.) Empirical values of the constants a_1 and a_2 of our equipment are in the vicinity of $a_1 \approx -0.4$ and $a_2 \approx 0.08$. However, the values of a_1 and a_2 are highly correlated, and therefore it is recommended to present at least one of them with a higher than the nominal accuracy of their determination (which is typically 5–10%).

Weights, statistical errors, and data simulation algorithm

In the interval of obtained count numbers, the probability of obtaining a particular pair of count numbers usually varies by many orders of magnitude. Consequently, the variance of the experimental distribution also has a strong dependence on the count numbers. To determine weights for least-squares fitting, one can assume for simplification that coordinates of particles in all counting intervals are randomly selected. (Thus we ignore correlations of the coordinates in consecutive counting intervals.) In this assumption, we have a problem with distributing M events over choices of different pairs of count numbers n_1, n_2, each particular outcome having a given probability of realization, $P(n_1, n_2)$. Covariance matrix elements of the distribution can be expressed as follows:

$$\langle \Delta P(n_1, n_2) \Delta P(n_1', n_2') \rangle = \frac{P(n_1, n_2)\delta(n_1, n_1')\delta(n_2, n_2') - P(n_1, n_2)P(n_1', n_2')}{M}, \quad (8)$$

where M is the number of counting intervals per experiment.

For a further simplification, one may ignore the second term on the right side of Eq. 8, which can be interpreted as a consequence of normalization. In this case, the weights are simply equal to the inverse values of the diagonal covariance matrix elements

$$W(n_1, n_2) = \frac{M}{P(n_1, n_2)}. \quad (9)$$

According to our experience, the weights given by Eq. 9 are sufficiently good for the purpose of parameter estimation. Also, the calculated values of χ^2 are usually close to unity. However, we have verified that the error values of estimated parameters returned by the linearized least-squares fitting algorithm are underestimated. The factor of underestimation is typically in the range of 1.5 to 4, depending most significantly on the ratio of the mean translational diffusion time of the molecule to the width of the counting time interval. The reason for the error underestimation is definitely the simplifying assumption behind Eq. 9, which ignores correlations between the photon count numbers measured in consecutive counting time intervals. As a reliable method of error determination, we have used the following algorithm. It involves, first, the simulation of a series of at least 30 random distributions at identical conditions; second, fitting them; and finally, the determination of statistical errors from scattered values of estimated parameters. The algorithm of data simulation does not ignore correlations between the photon count numbers of consecutive intervals, but includes random walk simulation of individual molecules. We have used this algorithm of error determination whenever error values are of special interest, despite its clumsiness and slowness. The error values presented in this paper are determined by this method. In other applications (in particular if the speed of analysis is of a higher interest than the exact error values), the error values corresponding to weights by Eq. 9 are often used multiplied by a roughly determined factor of underestimation.

Accuracy of 2D-FIDA versus 1D-FIDA

In Table 1 theoretical errors of FIDA and 2D-FIDA simulations are presented in two selected cases for two fluorescent species. In both cases the ratio of specific brightness values of the two species is three. Throughout the simulations, a data collection time of 8 s, a counting time interval of 40 μs, a diffusion time of 400 μs for both species, a speed of scanning (or flow) of 11000 $1/e^2$-radius values per second, and a background count rate of 1 kHz were assumed. Note that the statistical error values of the estimated parameters are significantly lower in the 2D-FIDA example. This result is related to the design principle of the two color experiments recommending that the spectral sensitivities of the two detectors (A and B) are tuned to different species. The values of parameters in the 2D-FIDA example are

TABLE 1 Theoretical errors of FIDA and 2D-FIDA as determined by simulations

Method	Parameter	Parameter value	Error, %
1D-FIDA	c_1V	0.5	11.1
	c_2V	0.5	6.6
	q_1	60 kHz	3.9
	q_2	20 kHz	14.0
2D-FIDA	c_1V	0.5	1.9
	c_2V	0.5	1.5
	q_{A1}	60 kHz	1.1
	q_{A2}	20 kHz	1.6
	q_{B1}	20 kHz	1.5
	q_{B2}	60 kHz	1.0

selected symmetrically. The error values would also be equal in pairs if the number of realizations was significantly higher than 30.

Two-dimensional moment analysis of fluorescence intensity fluctuations

In the same manner as one-dimensional FIDA can be generalized to the two-dimensional case, it can be done with MAFID. Factorial moments of the distribution $P(n_1, n_2)$ are defined as

$$F_{kl} = \sum_{n_1, n_2} \frac{n_1!\, n_2!}{(n_1 - k)!\, (n_2 - l)!} P(n_1, n_2). \tag{10}$$

Factorial moments are related to factorial cumulants K_{kl}

$$K_{kl} = F_{kl} - \sum_{\substack{i,j \\ i+j>0}} C_i^{k-1} C_j^{l} K_{k-i,l-j} F_{ij}. \tag{11}$$

where C denotes binomial coefficients. A simple relation can express cumulants through concentrations and specific brightness values

$$K_{kl} = \chi_{k+1} T^{k+1} \sum_i c_i q_{1i}^k q_{2i}^l. \tag{12}$$

If the unit of B is selected by the equation $\chi_1 = \chi_2$, χ_1 has the meaning of the sample volume, denoted by V, and Eq. 12 can be written as

$$\gamma_{k+1} K_{kl} = \sum_i (c_i V)(q_{1i} T)^k (q_{2i} T)^l. \tag{13}$$

where γ denotes a series of constants characterizing the brightness profile:

$$\gamma_m = \frac{\chi_l}{\chi_m}. \tag{14}$$

The principle of moment analysis is to determine values of a few cumulants from an experiment and solve a system of Eqs. 12 with respect to unknown concentrations and brightness values.

In Table 2 statistical errors of 2D-FIDA and 2D-MAFID are presented as determined by generating a series of 30 random distributions of count numbers, simulated for identical "samples," thereafter applying 2D-FIDA and 2D-MAFID and determining the variance of estimated parameters in both cases. It is evident that the advantages of 2D-FIDA compared to 2D-MAFID increase with the number of parameters to be estimated.

In Table 3 the relative deviation of mean values (i.e., bias) of estimated parameters are presented for 2D-FIDA and 2D-MAFID. In each case bias is determined from

TABLE 2 Statistical errors of 2D-FIDA and 2D-MAFID in a few selected cases

Data collection time, s	Number of species	Number of estimated parameters	Specification of cumulants used in 2D-MAFID	Specification of parameters	Parameter values	Error of 2D-FIDA, %	Error of 2D-MAFID, %
2	1	3	K_{01}	cV	0.5	1.5	1.6
			K_{10}	q_A	60 kHz	1.6	1.8
			K_{11}	q_B	40 kHz	1.8	1.9
8	2	4	K_{01}	c_1V	0.5	1.01	1.05
			K_{10}	c_2V	0.5	0.77	2.63
			K_{02}	q_{A1}	60 kHz	0.89	0.75
			K_{20}	q_{A2}	20 kHz	(fixed)	(fixed)
				q_{B1}	20 kHz	1.54	4.45
				q_{B2}	60 kHz	(fixed)	(fixed)
8	3	5	K_{01}	c_1V	0.2	2.6	3.4
			K_{10}	c_2V	0.2	1.5	1.8
			K_{02}	c_3V	0.2	2.4	2.8
			K_{11}	q_{A1}	40 kHz	1.9	3.0
			K_{20}	q_{A2}	20 kHz	(fixed)	(fixed)
				q_{A3}	60 kHz	(fixed)	(fixed)
				q_{B1}	10 kHz	5.4	8.2
				q_{B2}	60 kHz	(fixed)	(fixed)
				q_{B3}	70 kHz	(fixed)	(fixed)
8	2	6	K_{01}	c_1V	0.5	1.9	4.6
			K_{10}	c_2V	0.5	1.5	4.8
			K_{02}	q_{A1}	60 kHz	1.1	1.8
			K_{11}	q_{A2}	20 kHz	1.6	4.3
			K_{20}	q_{B1}	20 kHz	1.5	4.7
			K_{21}	q_{B2}	60 kHz	1.0	1.7

Error values were calculated from the scattered results of analysis applied to a series of simulated data (see text for details).

TABLE 3 Bias values of 2D-FIDA and 2D-MAFID

Parameter specification	Parameter value	Bias of 2D-FIDA, %			Bias of 2D-MAFID, %		
		Case 1	Case 2	Case 3	Case 1	Case 2	Case 3
c_1V	1.0	+0.1 ± 0.2	−0.35	−2.0	+0.1 ± 0.2	−6.5	−28
c_2V	0.05	+0.6 ± 0.4	−2.0	−10.6	+1.8 ± 0.6	−15.6	−69
q_{A1}	20 kHz	−0.1 ± 0.2	+0.8	+5.0	−0.3 ± 0.3	+10.0	+58
q_{A2}	100 kHz	−0.3 ± 0.4	−0.7	−11.2	−0.9 ± 0.3	+5.5	+41
q_{B1}	1 kHz	−1.2 ± 0.5	+2.6	+20.6	−6.7 ± 3.0	+75	+563
q_{B2}	200 kHz	−0.3 ± 0.4	+1.2	+1.3	−0.9 ± 0.3	+11.6	+99

In case 1, identical models were used in data simulation and analysis, while in cases 2 and 3, a less stringent model was used for analysis than in data simulation (see text for details).

analysis of a series of 30 simulated random distributions of count numbers. Three cases were analyzed. In the first case, models used in data simulations and data analysis were identical. In the second case, the distributions of count numbers were simulated assuming that particles of the second species are not equivalent, but are distributed by their individual brightness with a relative half-width of 20%. However, we intentionally ignored this phenomenon in analysis. Of course, applying a slightly inadequate model for analysis produces bias of estimated parameters. The third case is similar to the second one except that the relative half-width of the individual brightness distribution of the second species is 50%, which is a usual value for vesicular preparations. It is worth noting that methodological deviations are noticeable when mapping weighted residuals of 2D-FIDA in cases two and three. However, 2D-FIDA still returns meaningful results, while 2D-MAFID is much more sensitive to model deviations.

EXPERIMENTS

Equipment

The central optical part of a 2D-FIDA experiment is a confocal microscope as it is used in fluorescence correlation spectroscopy (Koppel et al., 1976). For excitation of fluorescence, a beam from a continuous-wave laser is attenuated by neutral filters, passes a beam expander, and is directed to the microscope objective by a dichroic mirror. In a number of experiments with slowly diffusing particles, e.g., vesicles, beam scanning in combination with sample scanning is used, as a tool known from laser scanning microscopy. Fluorescence is collected by the same objective through the dichroic mirror and is focused to a confocal pinhole, which serves to reject the out-of-focus light. The light, which passes the pinhole, is divided by a beamsplitter for detection by two detectors. Depending on the general type of a 2D-FIDA experiment, the beamsplitter is either a polarization cube or a dichroic mirror. In the first case, a common spectral band-pass filter is used, while in the case of two-color FIDA, each detector has a different band-pass filter positioned in front of it (Fig. 1). The photon counting detectors are silicon avalanche photodiode modules (SPCM-AQ-131, EG&G Optoelectronics, Vaudreuil, Quebec, Canada). The TTL pulses from the detectors are collected continuously by a two-channel counter constructed at EVOTEC as a computer plug-in card that calculates the count number distributions in real time from the 32 MB onboard buffer. By feeding the detector outputs to a correlator, FCS measurements can be performed in parallel with FIDA experiments.

The levels of background count rate for both detectors are determined in a separate experiment on bidistilled water. The main contributor to the nonfluctuating background light intensity is Raman scattering from water.

The radius of the monitored sample volume can be adjusted by selecting an appropriate expansion factor of the original laser beam. The focal beam radius of ~0.6 μm is used, yielding diffusion times for simple organic dye molecules (e.g., 5′-(6-carboxytetramethylrhodamine (TAMRA)) of ~260 μs, which is considered long compared to the 40 μs dwell time of counters, so that the assumption of constant molecular brightness during the counting interval is well-founded. The excitation intensity is adjusted as a compromise between a high count rate per molecule and low population of the triplet state. In our experiments we have kept the triplet state population below 15% because higher triplet population values might significantly distort the apparent spatial brightness profile (Kask et al., 1999).

Test experiments

For methodological test experiments two different dyes were selected, TAMRA and rhodamine red X (RRX). These dyes have different emission spectra and different extinction coefficients at the excitation wavelength of

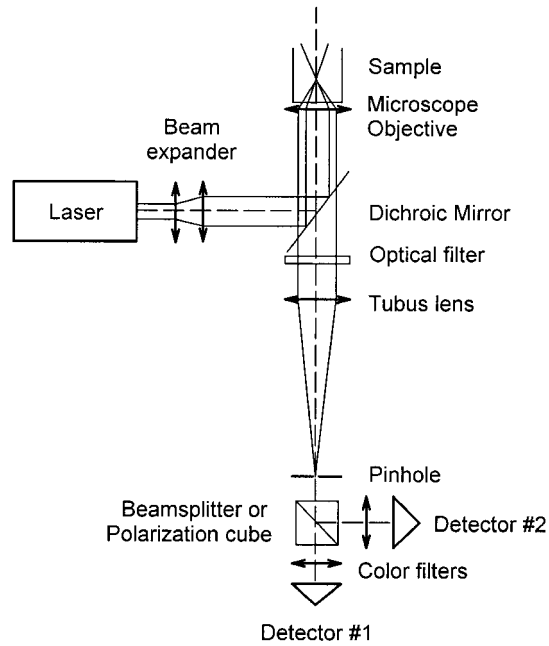

FIGURE 1 Schematic drawing of the optical set-up.

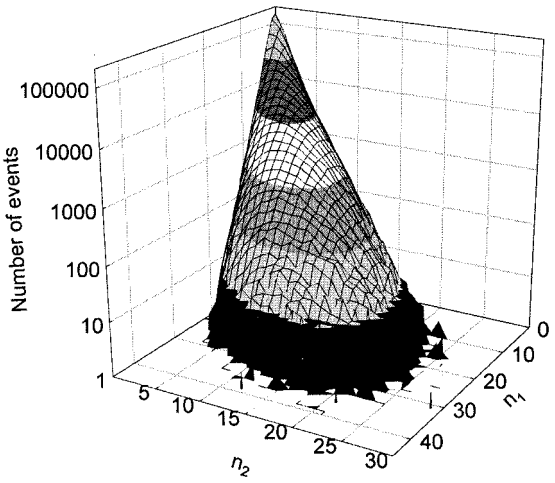

FIGURE 2 Graphical presentation of a joint distribution of the number of photon counts measured for a solution of TAMRA. The *z*-axis gives the number of events with a given pair of count numbers n_1 and n_2. Fitting of the distribution returns the mean number of particles, $cV = 1.139 \pm 0.004$, the specific brightness for the "red" channel $q_1 = 79.4 \pm 0.3$ kHz, and for the "yellow-green" channel $q_2 = 50.9 \pm 0.2$ kHz.

543.5 nm. In these experiments, a wideband 40/60 beamsplitter was used in front of the detectors. The spectral filter of the "red" channel has the central wavelength of 605 nm and FWHM of 50 nm, while the corresponding figures for the "yellow-green" channel are 575 nm and 30 nm. The dyes were diluted in distilled water so that the average number of molecules in the observation volume was in the range of 0.5–2.0, corresponding to concentrations between 0.23 and 0.92 nM. For each experiment ~20 μl of the sample solution was placed on a coverslip separating the sample from the water immersion objective (Zeiss C-Apochromat 40 × 1.2 W Korr). All the dyes were measured separately for 60 s, as were their mixtures with two different concentration ratios (~1:1 and 1:2.5). The parameters describing the spatial brightness profile were determined from adjustment experiments on TAMRA and were fixed for the subsequent analysis of other samples at values $a_1 = -0.405$ and $a_2 = 0.0772$.

Results of test experiments

As an example, Fig. 2 visualizes a joint count number distribution of an ~0.5 nM TAMRA solution. The results of the above-described test experiments are summarized for multiple realizations in Table 4. We have not specified samples by concentration values calculated from dilution factors of the preparation because adsorption of dye molecules to glass surfaces may influence the real concentrations in the sample volume. Therefore, the determined concentration values vary slightly from realization to realization. However, the specific brightness values are well-reproduced throughout all experiments.

It is worth noting that distributions measured with mixtures are qualitatively different from those measured for pure dyes. Fig. 3 visualizes weighted residuals of fitting a distribution measured with a mixture of TAMRA and RRX. The top graph (*A*) corresponds to the adequate analysis when two species were assumed to be present; residuals are scattered quite randomly and uniformly. The bottom graph (*B*) corresponds to the assumption that only a single species is present. Here a significant difference between the measured and the calculated distribution is evident.

TABLE 4 Results of 2D-FIDA applied to solutions of TAMRA, RRX, and their mixture

Sample	Number of realization	Mean number of molecules per sample volume, cV	Specific brightness in "red," q_1, kHz	Specific brightness in "yellow-green," q_2, kHz
TAMRA	1	1.128 ± 0.004	79.6 ± 0.3	51.3 ± 0.2
	2	1.139	79.4	50.9
	3	1.160	79.4	50.8
	4	1.171	79.0	50.6
RRX	1	1.892 ± 0.007	48.0 ± 0.2	15.63 ± 0.06
	2	1.859	48.0	15.63
	3	1.850	47.3	15.44
	4	1.811	47.9	15.58
TAMRA and RRX, (approx. 1:1)	1	0.99 ± 0.03	78.0 ± 0.8	51.8 ± 0.7
		1.14 ± 0.03	49.1 ± 0.5	15.0 ± 0.4
	2	1.01	76.8	51.1
		1.08	49.5	15.1
	3	0.99	77.9	51.8
		1.03	49.3	15.1
	4	0.97	76.9	51.7
		1.03	50.0	15.5
TAMRA and RRX, (approx. 1:2.5)	1	0.93 ± 0.03	74.6 ± 0.8	49.6 ± 0.9
		2.51 ± 0.04	47.6 ± 0.3	14.7 ± 0.2
	2	0.98	75.2	49.2
		2.38	46.8	14.2
	3	0.96	75.0	49.4
		2.25	48.0	14.7
	4	0.94	76.1	49.9
		2.16	47.6	14.8

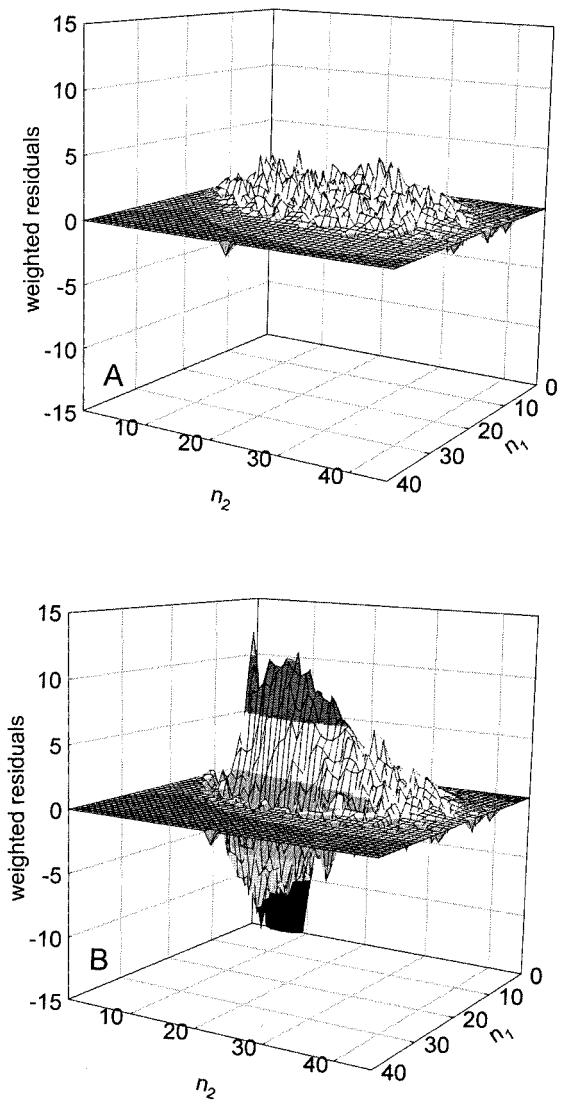

FIGURE 3 Graphical presentation of weighted residuals of a joint distribution of count numbers obtained from a mixture of TAMRA and RRX. The top graph (*A*) was obtained by assuming two fluorescent species to be present, while the bottom graph (*B*) corresponds to the wrong assumption of single species. n_1 is the count number obtained by the "red" detector, and n_2 is the count number obtained by the "yellow-green" detector.

APPLICATIONS

In the following section we shall present in detail two essentially different examples of 2D-FIDA from biochemical assay development illustrating the broad applications of the method. As outlined in the introduction of this paper it is essential that the two detectors monitor different qualities of fluorescent species. Therefore, in the first example the two detectors monitor the two polarization components of fluorescence, while in the second example the two detectors have different spectral responses, thus monitoring different labels.

Fluorescence polarization studies

In conventional fluorescence polarization studies, average intensities of two polarization components of fluorescence are directly measured. Fluctuations of the intensities are not of direct interest, but are considered rather as a source of statistical errors. The conventional fluorescence polarization method has proven to be a powerful tool in the study of molecular interactions (Checovich et al., 1995; Jameson and Sawyer, 1995; Jolley, 1996). Changes in the fluorescence polarization values of a sample containing a fluorescently labeled binding partner reflect changes in molecular volume and, hence, provide direct information on equilibrium binding. Fluorescence polarization measurements can also be performed in real time, allowing the kinetic analysis of association and dissociation reactions. One of the most widely used fluorescence polarization applications is the competitive immunoassay used for the detection of therapeutic and illicit drugs. The method of fluorescence polarization has been used for clinical immunoassays for more than a decade (Jolley, 1981). The homogeneous FPIA (fluorescence polarization in immunoassays) has well-accepted advantages over conventional heterogeneous immunoassays like RIA or ELISA. However, it fails if multiple-binding step reactions are to be investigated because the separation of individually polarized species is impossible. Therefore, ligand-binding curves demonstrate only the overall decrease of polarization, meaning that the mechanistic binding constants cannot be determined. Further limitations are seen in sample volume and in mass restrictions.

With 2D-FIDA the full content of information usually buried in fluorescence anisotropy can be used, thereby overcoming the limitations mentioned above. 2D-FIDA directly determines two specific quantities per fluorescent species in one measurement: the fluorescence intensity per molecule and the anisotropy of a given model. Based on this supplementary information, the delineation of all participating species and even the quantification of the binding behavior are possible. 2D-FIDA anisotropy is an ideal tool for the quantitative description of systems exhibiting multiple binding steps, aggregation, and multimerization phenomena as demonstrated with the following example.

The theophylline/anti-theophylline antibody interaction

Theophylline therapy has been a cornerstone of asthma therapy for several years and, therefore, there is a strong demand for assaying and fine-tuning the theophylline level in serum (Hinds et al., 1984; Poncelet et al., 1990; Mallin et al., 1990). To demonstrate the capabilities of 2D-FIDA we have investigated the binding of theophylline antigens to anti-theophylline antibodies from a polyclonal anti-theophylline serum (Europe Research Products, Cambridge, UK; Cat. no. RPCR2079R). This two step binding reaction can be described by the reaction scheme shown in the top part of Fig. 5. It assumes the existence of two identical but independent binding sites. The antigens were labeled with TAMRA using standard labeling procedures. They exhibited in classical FP analysis a low anisotropy value of 0.055 upon interacting with the antibody. Therefore they form a critical basis for illustrating the sensitivity of 2D-FIDA.

For the binding experiments the stock solutions of antibody and antigens were diluted in a PBS buffer with 0.05% Tween 20. After mixing the compounds, the mixture was incubated for 30 min at room temperature. Matching the spectral properties of the conjugates, the system was excited at the 543.5 nm line of an He/Ne laser (Uniphase, San Jose, CA, USA). As two examples, measured joint distributions of photon count numbers and results of 2D-FIDA applied to samples at different antibody dilution values but a constant ligand concentration of 2 nM are illustrated by Figs. 4 and 5. Antibody concentrations are in arbitrary units referring to effective dilutions. Water background was below 1 kHz in each detection channel.

Two-color approach of 2D-FIDA for vesicle-based binding assays

For the two-color approach of 2D-FIDA, the two detectors are spectrally tuned to monitor fluorescence from two labels of different color. In the assay type described below, ligand molecules are labeled in "green."

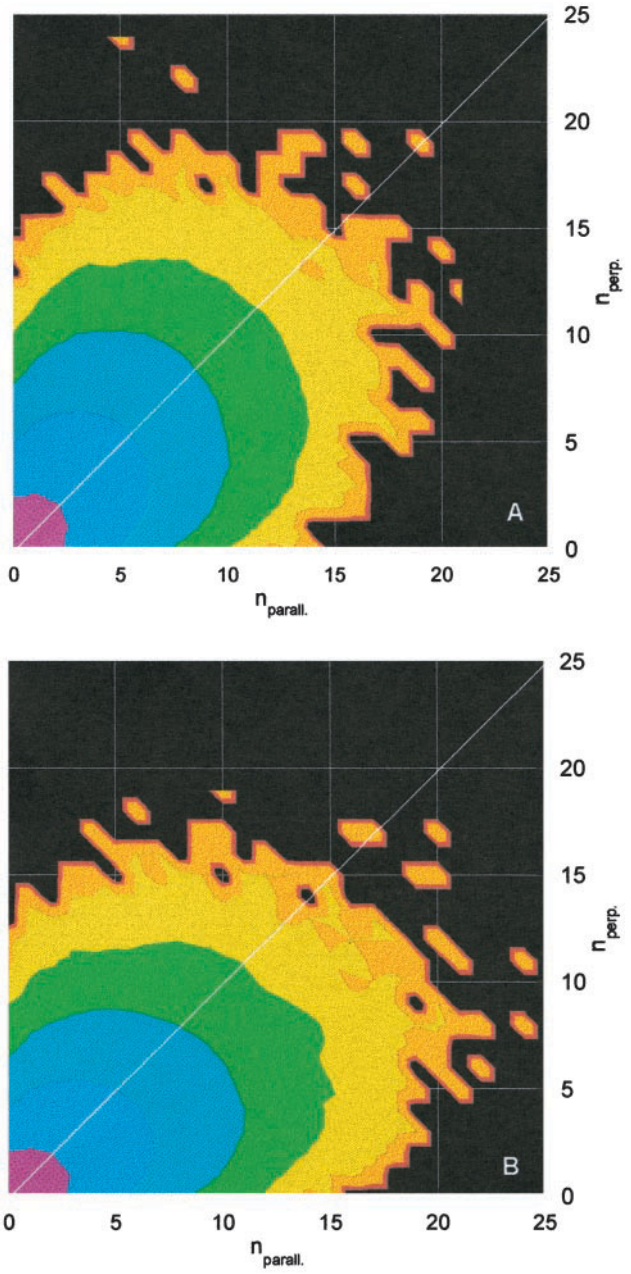

FIGURE 4 Maps of joint distributions of the numbers of photon counts for the "parallel" and "perpendicular" polarization components of fluorescence measured for equal theophylline concentrations of 2 nM, but different antibody concentrations. (*A*) Effective antibody dilution: 1:200,000; (*B*) effective antibody dilution: 1:10,000. Data acquisition time of each experiment was 120 s. Each of the colors covers an order of magnitude of the number of events.

Because each vesicle carries a large number of receptors, vesicles in samples with a low binding degree can be distinguished from vesicles in samples with a high binding degree by a significantly higher specific brightness in "green." Vesicles are additionally stained in "red." Specific brightness of vesicles in "red" is not altered by binding of ligand molecules, but staining in "red" is a means to increase contrast between free ligand molecules (which are nearly invisible in "red") and vesicles (which

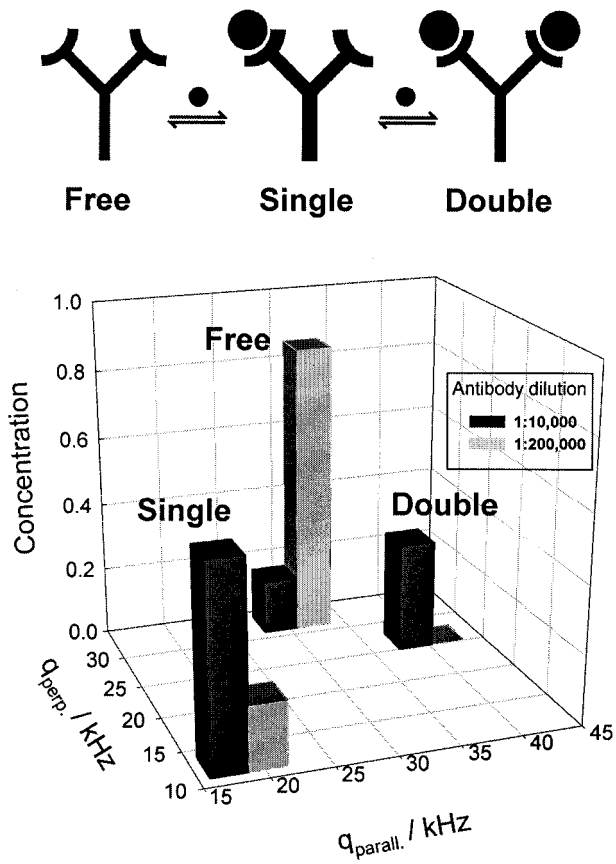

FIGURE 5 Two-step binding of theophylline antigens to anti-theophylline antibodies and results of 2D-FIDA applied to the data from Fig. 4. As a preliminary step of the analysis, the specific molecular brightness of free theophylline antigens was separately measured to be 30.7 ± 0.1 kHz and 32.5 ± 0.1 kHz in the "parallel" and the "perpendicular" detector, respectively. In the subsequent analysis, the pair of specific molecular brightness values of the single bound antigens was determined to be 18.8 ± 0.9 kHz and 12.6 ± 0.8 kHz, while for the doubly bound antigens the corresponding values were 40.3 ± 1.6 kHz and 26.5 ± 1.0 kHz. Pure statistical errors are presented here.

in the case of extremely low binding may be of nearly the same brightness in "green" as free ligand molecules). Contributions from the two fluorescent species of a single sample to the measured joint distribution of the numbers of photon counts are very different in this assay type indeed, and therefore the analysis is extremely reliable.

Binding of somatostatin-14 to the human type-2 high-affinity somatostatin receptor

To demonstrate the advantages of 2D-FIDA the binding of TAMRA-labeled somatostatin-14 (SMS–14–5TAMRA) to small membrane vesicles carrying the human type-2 high-affinity somatostatin receptor SSTR-2 (Schoeffter et al., 1995) was chosen as a biological test system. The top part of Fig. 7 illustrates the principle of the assay.

Membrane vesicles were prepared from CCL39 hsst2 cells overexpressing the receptor. The cells were disrupted in vesicle buffer [10 mM HEPES, pH 7.6 (KOH), 5 mM $MgCl_2$] in the presence of protease inhibitors [Complete™ EDTA free (Roche Diagnostics GmbH, Mannheim, Germany) according to manufacturer's instructions with additional 0.2

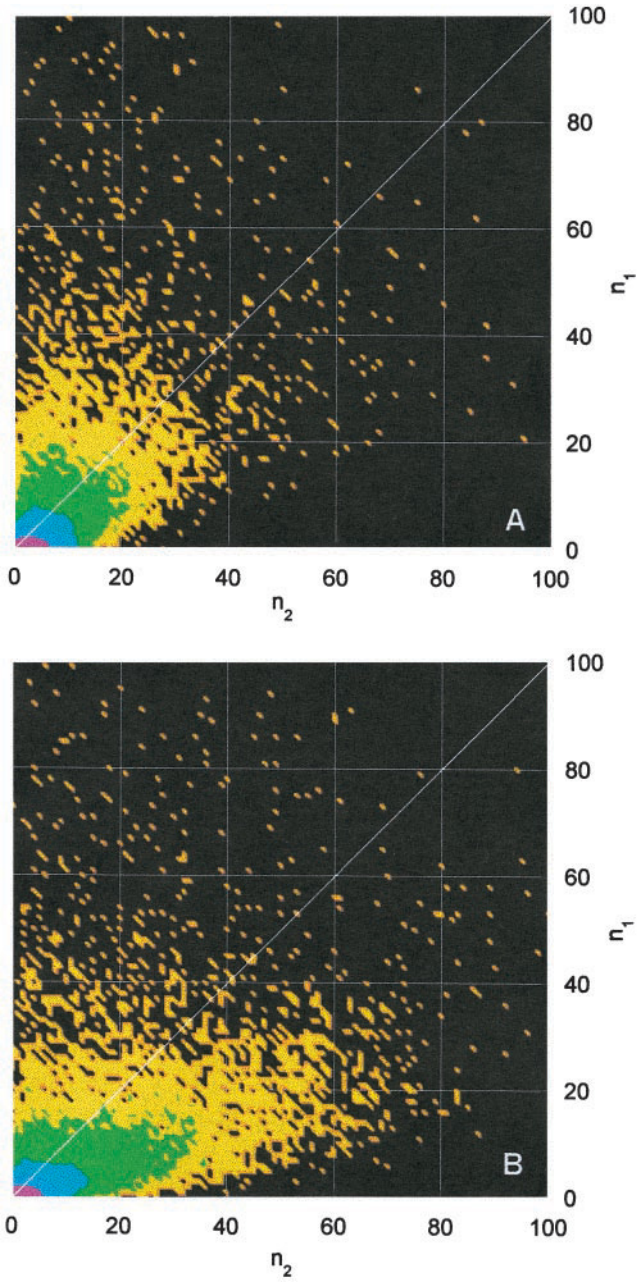

FIGURE 6 Maps of joint distributions of the numbers of photon counts in red (n_1) and green (n_2) measured under conditions of a low (A) and a high (B) degree of binding of SMS-14 to SSTR-2. Data acquisition time of each experiment was 8 s.

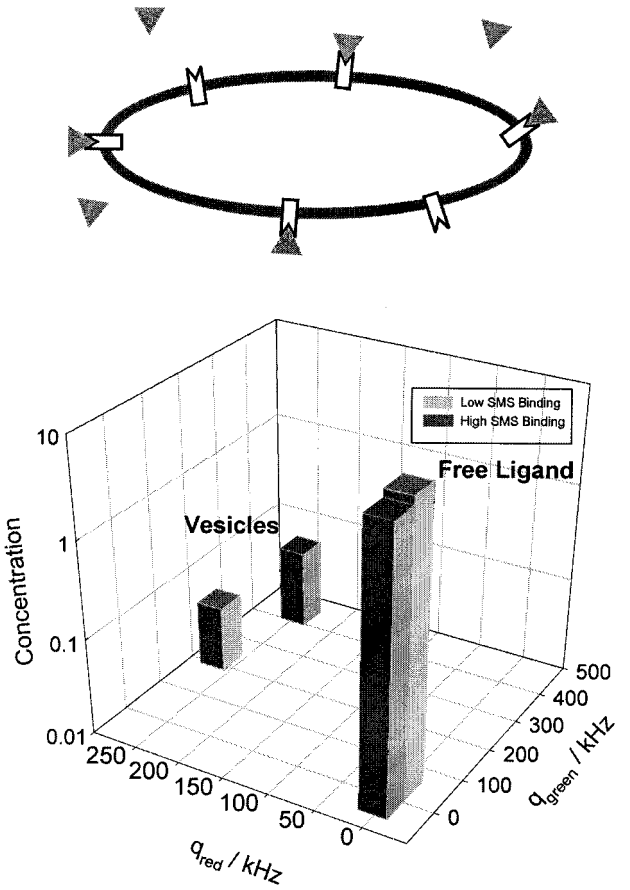

FIGURE 7 The principle of a two-color 2D-FIDA experiment with multiple binding sites per vesicle and results of 2D-FIDA applied to the data from Fig. 6. Free SMS-14 had a specific molecular brightness of 7.8 ± 0.2 kHz and 1.5 ± 0.03 kHz in the "green" and the "red" detector, respectively. The corresponding pair of values for the vesicles under high binding conditions was 427.3 ± 6 kHz and 247.0 ± 4 kHz, while under low binding conditions values of 216.9 ± 4 kHz and 270.2 ± 5 kHz were determined. The error values presented are statistical standard errors of a single two-component fit with six free parameters.

mg/ml soybean trypsin inhibitor and 0.5 mg/ml bacitracin] using a glass homogenizer (Dounce homogenizer). Cell nuclei and intact cells were removed by centrifugation at 900 × g for 5 min and the supernatant was recentrifuged at 48,000 × g for 30 min. After sedimentation the membranes were washed and resuspended in vesicle buffer and homogenized at maximum speed for 8 s using a Polytron homogenizer (Kinematica AG, Littau, Switzerland). Large particles were removed by centrifugation at 900 × g for 1 min and the supernatant containing small vesicles was used for binding experiments.

The receptor binding reaction was performed in vesicle buffer in the presence of protease inhibitors (see above), 0.01% (w/v) fluorosurfactant FC-135, 1.3% (v/v) DMSO and vesicles, corresponding to a total protein concentration of ~0.6 mg/ml, stained by 10 nM of the lipophilic tracer $DiIC_{18}(5)$ (Molecular Probes Europe BV, Leiden, The Netherlands).

For excitation of fluorescence of the two spectrally distinct labels, the 532-nm line of an Nd:Yag laser attenuated to 250 μW and the 632-nm line of a He-Ne laser attenuated to 25 μW were simultaneously used. To minimize misalignment of the two laser beams, they both passed through a single optical fiber before being focused by the microscope. An optical band-pass filter with a central wavelength of 590 nm, FWHM 60 nm, and another one with a central wavelength of 690 nm, FWHM 40 nm were used in front of the two detectors, monitoring fluorescence from the two labels separately. Because vesicles are slowly diffusing particles, in these experiments an area of 0.05 mm^2 of each sample was scanned, using sinusoidal beam scanning of 25 Hz frequency, 100 μm amplitude in one direction, and sample scanning of 500 μm per 8 s data collection time in the other direction.

In Fig. 6 two typical examples of count number distributions corresponding to a high and a low degree of binding are compared. In Fig. 6 A the vesicle-bound ligand (SMS-14–5TAMRA) was competed off by the addition of a large excess of nonfluorescent competitor [SRIF-14 (Sigma,

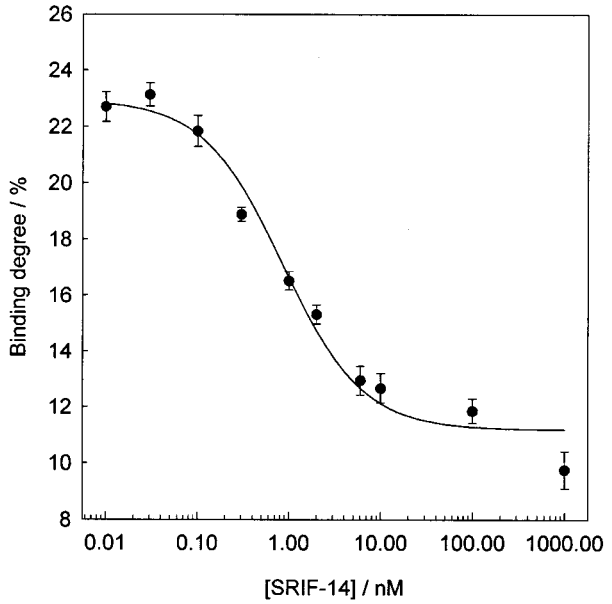

FIGURE 8 Competition of vesicle-bound SMS-14-5TAMRA by unlabeled SRIF-14.

Deisenhofen, Germany), 1 μM competitor, 3 nM total ligand]. It is clearly visible that the distribution obtained in the absence of competitor (Fig. 6 *B*) is more expanded in the n_2 direction than in the presence of competitor. The n_2 direction represents the green fluorescence of the labeled ligand and, hence, is a measure of the ligand binding.

Using a fit model that accounts for two different species, both the concentration (particle number in the confocal volume) and the fluorescence brightness values for the free ligand and the ligand bound to vesicles were obtained. The vesicles are well distinguished from the free ligand even in the presence of competitor (low binding). As expected, addition of competitor leads to a decrease in the green fluorescence of the vesicles and an increase in the concentration of free ligand (Fig. 7). The fact that the ligand does not completely dissociate from the vesicles is due to unspecific binding, which depends on the amount of vesicles used in the assay.

Next, we titrated the competitor from 1 μM down to 10 pM (10 measurements each) to record a dose-response curve and to determine the EC_{50} value. As shown in Fig. 8, 2D-FIDA analysis leads to a typical sigmoidal competition curve with very low standard deviations. The calculated EC_{50} value of 0.87 nM is in good agreement with EC_{50} values obtained using other evaluation methods (data not shown). Thus, it is not only possible to differentiate between high and low binding, but also small changes in the binding degree can be resolved with 2D-FIDA with high accuracy. This is of particular importance if one aims to identify assay inhibitors ("hits") in high throughput drug screening.

CONCLUSIONS

In this paper we extended the theory of fluorescence intensity distribution analysis (FIDA) to two dimensions. By comparing theoretical with experimental data we could prove that the collected joint photon count number distributions are in agreement with the theoretically predicted ones. The introduction of the generating function facilitates data evaluation and makes the method applicable even in high throughput drug screening, where it has already been successfully applied (EVOTEC/Novartis collaboration).

Compared to many other fluctuation methods, which often suffer from low precision, the presented method can be extremely accurate. In fact, the accuracy depends on the skill of assay design; a very important nuance is that fluorescence from different species was split at different intensity ratios. Only in the case of the worst design, when fluorescence from different species is split between the two detectors at the same ratio, is the resolving power of 2D-FIDA equal to that of 1D-FIDA. The higher the contrast between species in the intensity ratio, the more one can gain from using 2D-FIDA.

2D-FIDA has proven to be a method of versatile applicability. It offers new insights into polarization studies. Compared to a number of other polarization methods, it is superior due to its ability to separate different components and determine their absolute concentrations. Among different fluorescence methods we have compared with 2D-FIDA, only the polarization analysis by burst integrated fluorescence lifetime (BIFL; Schaffer et al., 1999) has both of these properties. However, BIFL is restricted to significantly lower concentrations than 2D-FIDA.

The other branch of 2D-FIDA, the two-color analysis, offers the possibility to work under near-to-ideality conditions because here assays can be designed or selected with a pronounced contrast between the bound and non-bound states. The closest method to two-color 2D-FIDA is its counterpart in FCS, the cross-correlation method. Between them, 2D-FIDA seems to be a more favorable method again, because FIDA is directly focused to separate the absolute concentrations of different components, whereas in FCS only the product of the concentration and the square of the specific brightness of each component can be directly separated.

The authors gratefully acknowledge NOVARTIS PHARMA AG for providing the SMS model. Dr. Nicholas Hunt is acknowledged for critically reading the manuscript.

REFERENCES

Checovich, W. J., R. E. Bolger, and T. Burke. 1995. Fluorescence polarization—a new tool for cell and molecular biology. *Nature.* 375: 254–256.

Chen, Y., J. D. Müller, P. T. So, and E. Gratton. 1999. The photon counting histogram in fluorescence fluctuation spectroscopy. *Biophys. J.* 77: 553–567.

Hinds, J. A., C. F. Pincombe, R. K. Kanowski, S. A. Day, J. C. Sanderson, and P. Duffy. 1984. Ligand displacement immunoassay: a novel enzyme immunoassay demonstrated for measuring theophylline in serum. *Clin. Chem.* 30:1174–1178.

Jameson, D. M., and W. H. Sawyer. 1995. Fluorescence anisotropy applied to biomolecular interactions. *Methods Enzymol.* 246:283–300.

Jolley, M. E. 1981. Fluorescence polarization immunoassay for the determination of therapeutic drug levels in human plasma. *J. Anal. Tox.* 5:236–240.

Jolley, M. E. 1996. Fluorescence polarization assays for the detection of proteases and their inhibitors. *J. Biomol. Screening.* 1:33–38.

Kask, P., K. Palo, D. Ullmann, and K. Gall. 1999. Fluorescence-intensity distribution analysis and its application in biomolecular detection technology. *Proc. Natl. Acad. Sci. USA.* 96:13756–13761.

Kask, P., P. Piksarv, and U. Mets. 1985. Fluorescence correlation spectroscopy in the nanosecond time range: photon antibunching in dye fluorescence. *Eur. Biophys. J.* 12:163–166.

Kask, P., P. Piksarv, M. Pooga, U. Mets, and E. Lippmaa. 1989. Separation of the rotational contribution in fluorescence correlation experiments. *Biophys. J.* 55:213–220.

Koppel, D. E., D. Axelrod, J. Schlessinger, E. L. Elson, and W. W. Webb. 1976. Dynamics of fluorescence marker concentration as a probe of mobility. *Biophys. J.* 16:1315–1329.

Magde, D., E. L. Elson, and W. W. Webb. 1972. Thermodynamic fluctuations in a reacting system—measurement by fluorescence correlation spectroscopy. *Phys. Rev. Lett.* 29:704–708.

Mallin, W., E. Eber, H. J. Semmelrock, and M. Zach. 1990. Determination of theophylline serum level: comparison between a rapid test (enzyme-immuno-chromatography) and conventional fluorescence polarization immunoassay. *Pneumologie.* 44:967–969.

Poncelet, S. M., J. N. Limet, J. P. Noel, M. C. Kayaert, L. Galanti, and D. Collet-Cassart. 1990. Immunoassay of theophylline by latex particle counting. *J. Immunoassay.* 11:77–88.

Qian, H., and E. L. Elson. 1990a. Distribution of molecular aggregation by analysis of fluctuation moments. *Proc. Natl. Acad. Sci. USA.* 87: 5479–5483.

Qian, H., and E. L. Elson. 1990b. On the analysis of high order moments of fluorescence fluctuations. *Biophys. J.* 57:375–380.

Schaffer, J., A. Volkmer, C. Eggeling, V. Subramaniam, G. Striker, and C. A. Seidel. 1999. Identification of single molecules in aqueous solution by time-resolved fluorescence anisotropy. *J. Phys. Chem.* 103: 331–336.

Schoeffter, P., J. Perez, D. Langenegger, E. Schupbach, I. Bobirnac, H. Lubbert, C. Bruns, and D. Hoyer. 1995. Characterization and distribution of somatostatin SS-1 and SRIF-1 binding sites in rat brain—identity with SSTR-2 receptors. *Eur. J. Pharmacol.* 289:163–173.

Schwille, P., F. J. Meyer-Almes, and R. Rigler. 1997. Dual-color fluorescence cross-correlation spectroscopy for multicomponent diffusional analysis in solution. *Biophys. J.* 72:1878–1886.